The Backfill Cycle of the Pressure Swing Adsorption Process

The backfill cycle in the pressure swing adsorption (PSA) separation of air to produce an enriched oxygen product using a zeolite 5A molecular sieve was studied theoretically and experimentally. The effects of the backfill cycle, cycle configuration, backfill rate, pressurisation rate, and product rate were studied. The theory agreed well with the experimental results in predicting the product oxygen concentration over a wide range of backfill pressures, thus giving a basic understanding of the bed dynamics of the backfill cycle. The theory showed that the backfill rate and adsorption capacity of the adsorbent were the most important parameters governing the efficiency of the PSA process. We showed that, given an adequate backfill pressure, a separate pressurization step could be omitted by incorporating it with the product release step with no detrimental effect on the product oxygen concentrations while increasing adsorbent productivity.

Jong-Leng Liow
C. N. Kenney
Department of Chemical Engineering
University of Cambridge
Cambridge CB2 3RA, England

Introduction

Pressure swing adsorption (PSA) is currently used to separate a wide range of gas mixtures, and the largest plants are those built for hydrogen purification. The largest number of units have been built for the separation of air to give either a nitrogen- or an oxygen-rich product; these units are generally small in size and many are portable. These smaller units have been gaining importance on the industrial scene in areas where the tonnage of the gas required is small, such as in waste water treatment, generation of medical oxygen, and nitrogen inert-gas blanketing.

There are three basic process steps necessary for the proper functioning of a PSA unit, being the pressurization, product release, and depressurization steps; these steps collectively constitute the simple cycle. The simple cycle suffers from the fact that its product concentration and recovery are low and are not suited for commercial operation. A number of extra process steps are included in a PSA process to increase the product concentration and recovery, for example, the purge, bed equalization, and backfill steps. The purge step has been studied extensively (Ruthven, 1984; Yang, 1987; Shin and Knaebel, 1987, 1988; Wankat, 1986) and involves the countercurrent passage of product through the adsorption bed at a lower pressure than the feed gas mixture. Hitherto, the backfill step has not been studied in detail. This step involves the pressurization of the adsorption bed with the product in a direction opposite to that of the feed gas mixture. Commercial units favor the backfill step, rather than the use of a portion of product gas, to supplement the feed gas mixture when only one gas component is being recovered as this involves much less piping and equipment capital cost. For a bed equalization step, the product or feed ends of two beds are linked with each other. One bed is at a higher pressure than the other, and the pressures in the two beds are allowed to equilibrate.

Skarstrom (1963) used the product to repressurize the bed in a PSA process separating hydrogen from hydrocarbons using activated carbon. The use of the backfill step in a two-bed process allowed product to be obtained while the other bed was being partially repressurized in contrast with the bed pressure equalization step which is preferably used only in processes employing three or more beds.

Flores-Fernandez and Kenney (1983) showed that the formation of an oxygen-rich zone during the pressurization step was crucial to the PSA operation. Kirkby and Kenney (1987) carried out theoretical modeling and experimental studies on the backfill step showing that there was no clear optimum backfill pressure above $P_b/P_f = 0.53$, where the product concentration and yields were not affected by increasing the P_b/P_f ratio. The product concentrations obtained were only slightly higher than for a purge cycle, but the yields were substantially higher. The equilibrium model they proposed was able to predict the trends.

Correspondence concerning this paper should be addressed to J.-L. Liow who is presently at the Department of Chemical Engineering, University of Melbourne, Parkville, Victoria, Australia, 3052.

Kayser and Knaebel (1988) studied the effect of combining the pressurization and product release steps on product recovery using an equilibrium model for a purge cycle. They found that the product recovery was always reduced compared to a conventional purge cycle, but more so if the adsorbent selectivity was low. However, Kirkby and Kenney (1987) showed that the simultaneous use of the backfill and purge steps kept product recoveries and concentrations high, indicating that it would therefore be possible that the backfill step could maintain the product concentration and recovery when the pressurization and product release steps are combined.

The present paper examines the importance of process rates, adsorbent characteristics and sequencing of the process steps on the performance of the backfill cycle in the separation of air to produce an oxygen-enriched product. The process rates include the rates of pressurization, backfill and product release. Two backfill cycles are considered: one, in which the pressurization and product release steps are separate; the other, in which they are combined. The effects are characterized by the product concentration of the cycle at steady state, and the experimental results are compared with the predictions of a mass transfer model.

Apparatus

The apparatus used, as illustrated in Figure 1, consisted of two stainless steel columns of 1 m in length and 0.073 m in ID, which were filled with zeolite 5A molecular sieve (ZMS). The columns can be operated either separately or together depending on the PSA cycle being studied. The feed gas consisted of air dried to 2 ppm water with CO_2 removed during the drying, which was fed in through a 0.0254-m-ID pipe. The feed gas contained N_2 (78.12 vol. %), O_2 (21.00 vol. %) and Ar (0.88 vol. %). Argon adsorption on ZMS is essentially identical to oxygen from 0 to 60°C and up to 5 bar. The O_2—Ar pair has been treated as a single component. The valves used for controlling the gas flow were VALVNUT single acting, normally closed pneumatic ball valves. Such valves have not been normally used for PSA operations; however, the fast response of these valves were found to be suitable for this study, the complete closing or opening of the valve taking a second at most. Each ball valve executed an average of 200,000 cycles each before repair of the seals was needed. The switching of the ball valves was controlled by a M6800 microchip board computer linked to a PDP11/45 computer, and activation was through solenoid and exhaust valves. The flow rates were controlled by diaphragm valves which were preset before the experiments. The product oxygen was measured with a Servomex oxygen analyzer which gave a continuous reading. Discrete readings for a cycle were averaged to give the product oxygen concentration for each cycle. At the start of an experiment, feed air was used to purge both beds at the lower operating pressure, this being atmospheric.

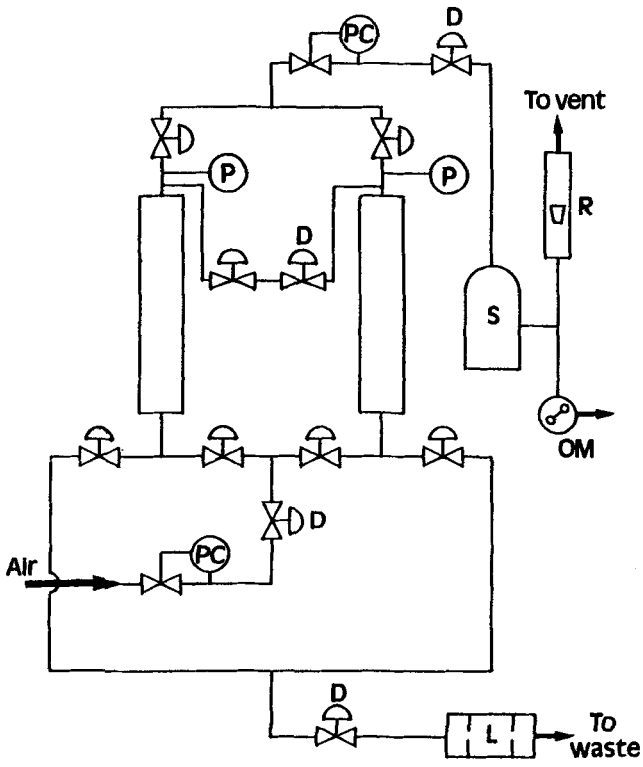

Figure 1. Experimental apparatus used.

D – diaphragm valves *PC* – pressure controller
L – silencer *R* – rotameter
OM – oxygen meter *S* – storage tank
P – pressure gauge

Adsorbents

The adsorbent used was a K155S 5A zeolite which was supplied regenerated and ready for use. The zeolite was selected from a batch of almost spherical particles and screened to a size fraction between 2.8 and 4.0 mm in diameter. The fraction was heated to 540 K for 10 hours to ensure that the batch was not contaminated before being packed into the adsorbent beds. The adsorption isotherms of oxygen and nitrogen at two different temperatures are shown in Figure 2. The intraparticle pore size

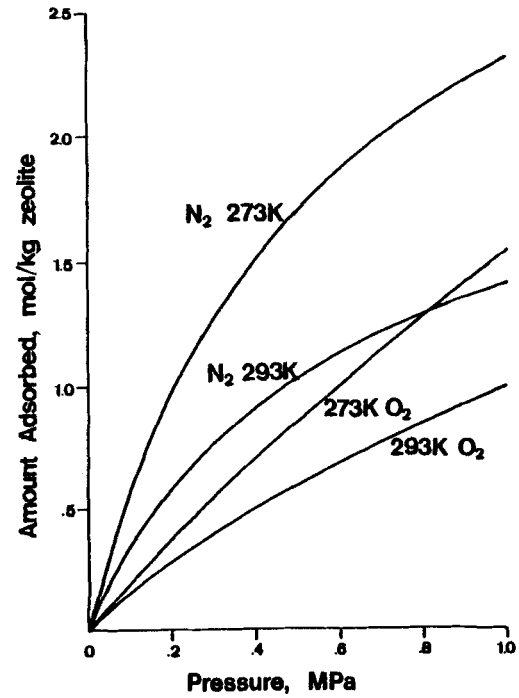

Figure 2. Adsorption isotherms of nitrogen and oxygen for the K155S 5A zeolite molecular sieve.

distribution (100–10,000 Å) was measured using mercury porosimetry and the results are shown in Figure 3. A unique feature of this adsorbent is the lack of pores between 100–1000 Å. The average pore size was calculated to be 8,000 Å. This indicated that the macropore channels within the particles were large, and bulk diffusion would predominate. The effective diffusion coefficients of oxygen and nitrogen in the 5A zeolite were measured using a Wicke-Kallenbach type apparatus (Liow, 1986) giving values corresponding to bulk diffusion through a fairly open pore structure. The effective diffusion coefficients were weakly dependent on the partial pressure of nitrogen in the diffusing gas as well as varying from one particle to another. The effective diffusion coefficients were assumed to vary inversely with pressure. The BET method showed that the bulk of the micropores were 5 Å in size with little in the 6–200 Å range. Table 1 lists some of the physical properties of this 5A zeolite.

The internal structure of the zeolite was observed with a scanning electron microscope (SEM). The crystal size varied from 3 to 10 μm in diameter and were irregular in shape. The crystals were bound in a fairly open pore structure where visual examination indicated a substantial proportion of them were over a micron in diameter. The crystals were fused together with no evidence of binder being used. Cylindrical rods were found to be scattered throughout the whole pellet, with diameters of 1 to 10 μm and lengths of 30 to 300 μm. The rod surfaces were clean and smooth with few zeolite crystals attached. An X-ray fluorescence analysis of the rods showed that they were composed of calcium aluminosilicate. It is suggested that the rods present in the pellets have been added during the manufacturing process to strengthen the material as the 5A zeolite is resistant to attrition and is able to withstand higher crushing loads than a number of commercial 5A zeolites available, such as Linde 5A and Laporte 5A zeolites.

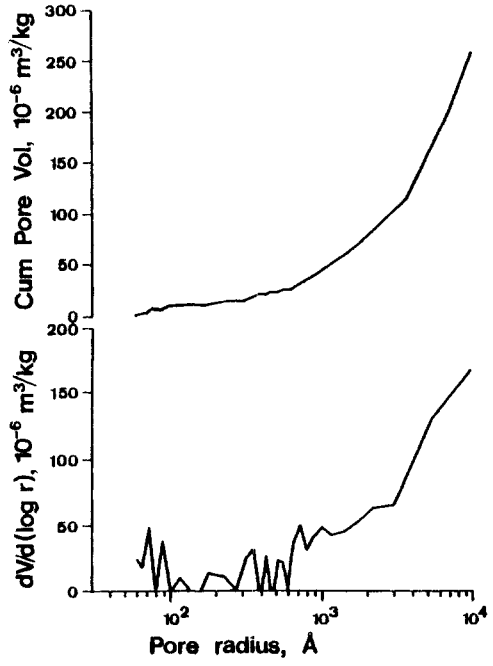

Figure 3. Pore size distribution and cumulative pore volume for the K155S 5A zeolite molecular sieve measured by mercury porosimetry.

Table 1. Physical Properties of the K155S 5A Zeolite

Bulk density, kg·m^{-3}	722
Bead density (Hg method of 100 kPa), kg·m^{-3}	1,164
Crystal density (benzene method at 100 kPa), kg·m^{-3}	1,639
Solid density (water method at 100 kPa), kg·m^{-3}	2,534
Interparticle volume, m^3·kg^{-1}	5.26×10^{-4}
Macropore volume, m^3·kg^{-1}	2.48×10^{-4}
Micropore volume, m^3·kg^{-1}	2.25×10^{-4}
Macropore porosity	0.29
Micropore porosity	0.25
Pore size (Hg porosimetry), Å	7,980
Effective diffusivity, m^2·s^{-2}	4×10^{-6}
Oxygen Langmuir isotherm, C_T, mol·kg^{-1}	2.70
Oxygen Langmuir isotherm b, m^2·N^{-1}	5.15×10^{-7}
Nitrogen Langmuir isotherm C_T, mol·kg^{-1}	2.10
Nitrogen Langmuir isotherm b, m^2·N^{-1}	1.8×10^{-7}

Process Steps

The two backfill cycle configurations studied are shown in Figure 4 with the sequencing of the process steps. Configuration B1 shows a standard backfill cycle where all the process steps are separate while configuration BT1 shows a backfill cycle with

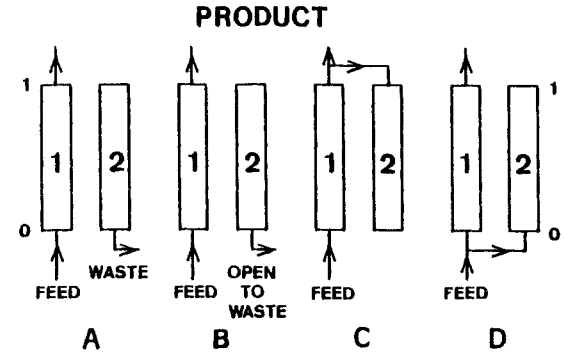

Bed CONFIGURATION B1

1	Product Release				Depress. Null BF Press.	
2	Depress.	Null	BF	Press.	Product Release	
	A	B	C	D		

Bed CONFIGURATION BT1

1	Press. + Product Release			Depress. Null BF	
2	Depress.	Null	BF	Press. + Product Release	
	A	B	C		

Press. Pressurisation
Depress. Depressurisation
BF Backfill

Figure 4. Sequencing of the backfill configurations B1 and BT1.

A, B, C, and D in the sequence correspond to those in the diagram and the dimensionless bed length is shown without the bed.

the pressurization and product release steps merged together. The null step was used to fill in the extra time present in runs that had different backfill pressures but an identical time period for the product release step. This set-up allowed the period of the product release step to be kept constant to give runs of similar product amounts for comparison when other parameters were varied. During the null step, the bed was left open to the waste line. The rate at which the bed was brought to the final pressure of a pressurization or backfill step was regulated by a diaphragm valve. This was possible because the large macropore size of the adsorbent allowed the gas-phase pressures within and without the adsorbent to reach equilibrium quickly. Varying the rate of pressure change allows one to obtain the value at which diffusion control becomes important for the process. For both the experimental runs and theoretical simulations, the feed for the backfill step was a time-varying product, and no attempt was made to homogenize the product. The product used corresponded to the time it was produced as shown in Figure 4.

Mathematical Model

The mathematical model proposed to simulate the experimental results makes a number of assumptions, the important ones being:

1. Gas behavior is ideal.
2. Bed packing characteristics are uniform with spherical particles.
3. Process is isothermal.
4. Weight change of adsorbent due to adsorption is negligible.
5. Temperature, pressure and concentration conditions have the same values at all points on the surface of a given particle.
6. There is no spatial pressure gradient.
7. Radial diffusion and wall effects are negligible.

The nonisobaric and isobaric steps have been treated separately in this model formulation as the zeolite 5A used had a unique property in than its average pore size was very much larger than that found in many commercially available zeolite 5A. With such a large average pore size, the pressure difference between the bulk gas phase and inside the particle would be small and it is reasonable to assume that the bulk gas would be forced into the particle by the changing pressure so that the film and diffusion mass transport resistance for the particle would be swamped by the bulk-phase flow of gas due to a changing pressure.

Pressure changing step

Consider an element of thickness Δz along a PSA bed. The flow into the element by bulk flow and axial dispersion is balanced by bulk flow, axial dispersion, accumulation within the void spaces, and adsorption onto the adsorbent. The mass balance for component i is:

$$\frac{\partial y_i}{\partial t} = -\frac{v}{\epsilon_t}\frac{\partial y_i}{\partial z} - \frac{y_i}{\epsilon_t}\frac{\partial v}{\partial z} + \frac{1}{\epsilon_t}\frac{\partial}{\partial z}\left(D_A\frac{\partial y_i}{\partial z}\right) - \frac{y_i}{P}\frac{\partial P}{\partial t} - \frac{wRT}{\epsilon_t P}\frac{\partial q_i}{\partial t}, \quad (1)$$

$$\frac{\partial q_i}{\partial t} = k_i(q_i^* - q_i),$$

$$\epsilon_t = \epsilon_b + (1 - \epsilon_b)\epsilon_p, \quad (2)$$

where q_i^* is the equilibrium amount that would be adsorbed on the surface for a given gas-phase concentration and q_i is the actual amount adsorbed on the surface. The rate constants k_i for nitrogen and oxygen are largely lumped constants for diffusion and adsorption in the zeolite microcrystallites. The velocity profile from the overall mass balance is given by:

$$\frac{\partial v}{\partial z} = -\frac{\epsilon_t}{P}\frac{\partial P}{\partial t} - \frac{wRT}{P}\sum_{k=1}^{n}\frac{\partial q_k}{\partial t}. \quad (3)$$

Equation 1 can then be rewritten as:

$$\frac{\partial y_i}{\partial t} = -\frac{v}{\epsilon_t}\frac{\partial y_i}{\partial z} + \frac{1}{\epsilon_t}\frac{\partial}{\partial z}\left(D_A\frac{\partial y_i}{\partial z}\right) + \frac{wRT}{\epsilon_t P}\left(y_i\sum_{k=1}^{n}\frac{\partial q_k}{\partial t} - \frac{\partial q_i}{\partial t}\right). \quad (4)$$

The boundary and initial conditions used depend on the physical nature of each step. However, two initial conditions are common to all pressure changing steps:

$$y_i = y_{i_{|\text{initial}}} \quad t_s = 0, \quad (5)$$

$$q_i = q_{i_{|\text{initial}}} \quad t_s = 0. \quad (6)$$

For the pressurization and backfill steps (during the backfill step, the collocation points for the bed are reversed so that the computer codes for the pressurization step can be used), the boundary conditions are:

Inlet:

$$\frac{\partial y_i}{\partial z} = -\frac{v}{D_A}(y_{i_{|z=0}} - y_{i_{|z=0^+}}) \quad z = 0, t_s \geq 0, \quad (7)$$

Closed end:

$$\frac{\partial y_i}{\partial z} = 0 \quad z = L, t_s \geq 0, \quad (8)$$

$$v = 0 \quad z = L, t_s \geq 0. \quad (9)$$

For a pressurization step with product release occurring concurrently, Eq. 9 changes to:

$$v = v_{\text{out}} \quad z = L, t_s \geq 0. \quad (10)$$

For the depressurisation step:

$$\frac{\partial y_i}{\partial z} = 0 \quad z = 0, t_s \geq 0, \quad (11)$$

$$\frac{\partial y_i}{\partial z} = 0 \quad z = L, t_s \geq 0, \quad (12)$$

$$v = 0 \quad z = L, t_s \geq 0. \quad (13)$$

Isobaric step

Let N_i be the molar flux of i into the particle with respect to fixed coordinates. The mass balance for component i in the bulk

gas phase is:

$$\frac{\partial y_i}{\partial t} = -\frac{v}{\epsilon_b}\frac{\partial y_i}{\partial z} + \frac{1}{\epsilon_b}\frac{\partial}{\partial z}\left(D_A \frac{\partial y_i}{\partial z}\right) + \frac{3RT(1-\epsilon_b)}{\epsilon_b R_o P}\left(N_i - y_i \sum_{k=1}^{n} N_k\right). \quad (14)$$

The velocity profile is given by

$$\frac{\partial v}{\partial z} = \frac{3RT(1-\epsilon_b)}{R_o P}\sum_{k=1}^{n} N_k. \quad (15)$$

Consider a spherical section of thickness Δr at a distance r from the center of a spherical particle. A mass balance requires the flux into the section at r to be equal to the flux out of the section at $r + \Delta r$, accumulation in the void spaces in Δr, and adsorption onto the adsorbent in Δr. The mass balance for component i is:

$$\frac{1}{r^2}\frac{d(r^2 N_i)}{dr} + \epsilon_p \frac{dC_i}{dt} + \rho_p \frac{dq_i}{dt} = 0. \quad (16)$$

Defining the particle volume average quantities for the adsorbed species concentration and the gas-phase concentration as:

$$\bar{q}_i = \frac{3}{R_o^3}\int_0^{R_o} q_i r^2\, dr, \quad (17)$$

$$\bar{C}_i = \frac{3}{R_o^3}\int_0^{R_o} C_i r^2\, dr, \quad (18)$$

and integrating Eq. 16 over the whole particle gives:

$$\epsilon_p \frac{d\bar{C}_i}{dt} + \frac{3}{R_o} N_{i|_{r=R_o}} + \rho_p \frac{d\bar{q}_i}{dt} = 0. \quad (19)$$

The overall mass balance is given by:

$$\epsilon_p \frac{d\bar{C}}{dt} + \frac{3}{R_o} N_{T|_{r=R_o}} + \rho_p \sum_{k=1}^{n} \frac{d\bar{q}_k}{dt} = 0. \quad (20)$$

The flux with respect to the local molar averaged velocity (J_i) is given by:

$$J_i = N_i - x_i N_T. \quad (21)$$

Substituting Eqs. 20 and 21 into Eq. 19 gives:

$$\frac{d\bar{x}_i}{dt} = \left[\rho_p\left(x_i \sum_{k=1}^{n}\frac{d\bar{q}_k}{dt} - \frac{d\bar{q}_i}{dt}\right) - \frac{3}{R_o} J_{i|_{r=R_o}}\right]\frac{RT}{\epsilon_p P}, \quad (22)$$

where

$$\bar{C} = \frac{P}{RT}. \quad (23)$$

For the isobaric diffusion of a gas mixture without any reaction, Graham's relation must be satisfied (Jackson, 1977), the relation being:

$$\sum_{i=1}^{n} N_i/\sqrt{M_i} = 0. \quad (24)$$

It is assumed that the bulk flow through the particles is solely due to the adsorption and desorption effects occurring within the adsorbent particles and these two quantities can be equated together to give:

$$N_i^b = -\frac{\rho_p R_o}{3}\frac{d\bar{q}_i}{dt}, \quad (25)$$

where N_i^b is the bulk flux for component i. This assumption is reasonable for the isobaric case. Fluxes are additive, so the total flux due to the bulk and diffusive fluxes is given by

$$N_i^T = N_i^D + N_i^b. \quad (26)$$

The Stefan-Maxwell relationship is used to relate the diffusion of component i in the particle to the fluxes of all the components present (labeled s) through the following relationship:

$$\frac{N_i^D}{D_{ki}} + \sum_{s\neq i}\frac{x_s N_i^D - x_i N_s^D}{D_{bi,s}} = -\frac{1}{RT}\nabla P_i, \quad (27)$$

where D_k and D_b are the Knudsen and bulk diffusion coefficients. Substituting Eqs. 25 and 26 into Eq. 27 gives the following:

$$\frac{N_i}{D_{ki}} + \sum_{s\neq i}\frac{x_s N_i - x_i N_s}{D_{bi,s}} = -\frac{1}{RT}\nabla P_i - \frac{\rho_p R_o}{3D_{ki}}\frac{d\bar{q}_i}{dt} - \frac{\rho_p R_o}{3}\sum_{s\neq i}\left[\frac{x_s\frac{d\bar{q}_i}{dt} - x_i\frac{d\bar{q}_s}{dt}}{D_{bi,s}}\right]. \quad (28)$$

The above equations give the fluxes at the surface of the particle. The Knudsen diffusion coefficient can be estimated from kinetic theory (Bird *et al.*, 1960). The initial conditions for all isobaric steps are Eqs. 5 and 6. For the product release step the boundary conditions are:

Inlet:

$$\frac{\partial y_i}{\partial z} = -\frac{v}{D_A}(y_{i|_{z=0}} - y_{i|_{z=0^+}}) \quad z = 0,\ t_s \geq 0, \quad (29)$$

Outlet:

$$\frac{\partial y_i}{\partial z} = 0 \quad z = L,\ t_s \geq 0, \quad (30)$$

$$v = v_{\text{product}} \quad z = L,\ t_s \geq 0. \quad (31)$$

For the purge step, the boundary conditions are:

Inlet:

$$\frac{\partial y_i}{\partial z} = -\frac{v}{D_A}(y_{i|_{z=0}} - y_{i|_{z=0^+}}) \quad z = 0,\ t_s \geq 0, \quad (32)$$

$$v = v_{feed} \quad z = 0, t_s \geq 0, \tag{33}$$

Outlet:

$$\frac{\partial y_i}{\partial z} = 0 \quad z = L, t_s \geq 0. \tag{34}$$

For a null step in which the bed does not perform any operation, the boundary conditions are similar to those for the depressurization step as the bed is left open to the waste stream and at the lower operating pressure.

Numerical Solution of the Model

The above bulk-phase concentration partial differential equations (Eqs. 1 and 14) were reduced using orthogonal collocation to a set of ordinary differential equations at selected points along the PSA bed which corresponded to the roots of the orthogonal polynomial used. The velocity equations (Eqs. 3 and 15) were reduced to a set of algebraic equations using orthogonal collocation which were solved by standard matrix methods. The fluxes in Eq. 28 were solved as a set of algebraic equations. The formulation and application of this method are fully described by Villadsen and Michelsen (1978). The partial differential equation (Eq. 2) relating to the rate of adsorption reduces to an ordinary differential equation at each collocation point. The ordinary differential equations were then solved using the Runge-Kutta-Merson method.

The axial dispersion was estimated by the equation proposed by Langer et al. (1978), being

$$D_A = \tau D'_{b1,2} + \frac{\mathrm{Pe}_\infty^{-1} v d_p}{1 + \dfrac{\beta' \tau D'_{b1,2}}{v d_p}}, \tag{35}$$

where $D'_{b1,2}$ is the bulk diffusivity of component 1 in 2 and is estimated using the Chapman-Enskog kinetic theory (Bird et al., 1960). The bulk diffusivity varies inversely with the bed pressure. The reciprocal axial tortuosity factor, τ, represents the ratio of the axial distance travelled between two cross-sections of a column to the true distance travelled by flowing molecules due to their zig-zag motion between solid particles. This was correlated (see Langer et al., 1978) as:

$$\tau = 0.45 + 0.55\epsilon_b. \tag{36}$$

The term $\beta'\tau D'_{b1,2}$ accounts for the effect of radial dispersion on the concentration gradient caused by axial dispersion, and a value of 8 was used for β' which represents a highly random walk situation. The limiting Peclet number, Pe_∞, is a function of the size of the particles in the packed bed;

$$Pe_\infty = 670 d_p \quad d_p < 0.003 \text{ m}, \tag{37}$$

$$Pe_\infty = 2.0 \quad d_p \geq 0.003 \text{ m}, \tag{38}$$

where d_p is the particle diameter.

The Langmuir adsorption isotherms were used to represent the pure component adsorption of oxygen and nitrogen. The form used is:

$$q_i^* = \frac{C_T b_i P_i}{1 + b_i P_i}. \tag{39}$$

Coadsorption was accounted using the ideal adsorbed solution (IAS) theory of Myers and Prausnitz (1965). Sorial (1983) has shown that the theory accounts satisfactorily for the binary adsorption equilibria of oxygen and nitrogen in zeolite 5A. The IAS theory requires the simultaneous solution of the following equations which necessitates the use of an iterative procedure.

The surface pressure for each component:

$$P_i^o(\pi) = \frac{(1 + b_i P_i)^{C_{Ti}/C_{Ti}} - 1}{b_i}, \tag{40}$$

The surface mole fraction concentration:

$$s_i = P x_i / P_i^o(\pi), \tag{41}$$

Mole fraction constraints:

$$\Sigma x_i = 1, \tag{42}$$

$$\Sigma s_i = 1. \tag{43}$$

The pressure variation with time was fitted to a linear variation for the pressurization and backfill steps and to an exponential variation for the depressurization steps where:

$$\frac{\partial P}{\partial t} = K(P_f - P_i)e^{-Kt}. \tag{44}$$

Results and Discussion

Orthogonal collocation

The Jacobi orthogonal polynomials were used in this work and are defined as:

$$\int_0^1 z^\beta (1 - z)^\alpha z^j \mathcal{P}_N^{\alpha,\beta}(z)\, dz = 0 \quad j = 0, 1, \ldots, N - 1. \tag{45}$$

With α and β both zero, the polynomials gave rise to a subset known as the Legendre polynomials. It was found that varying the values of α and β had little effect on the steady-state solution of a PSA cycle given a fixed number of interior collocation points. On keeping α and β both zero, increasing the number of collocation points gave increasing accuracy in the steady-state solution. The computational time doubled for each increase of 4–5 collocation points as the ODE's generated became progressively stiffer. Figure 5 shows for a given run, the difference in the steady-state oxygen concentration between different numbers of interior collocation points and one of 25 points. The differences fall very rapidly, and by 18 collocation points the difference is insignificant when compared to the accuracy obtainable with a reasonable oxygen measuring device. It was decided that 13 interior collocation points would be adequate to reasonably represent the results of the PSA cycle accurately. Figure 5 also shows that the differences were positive for an even number of

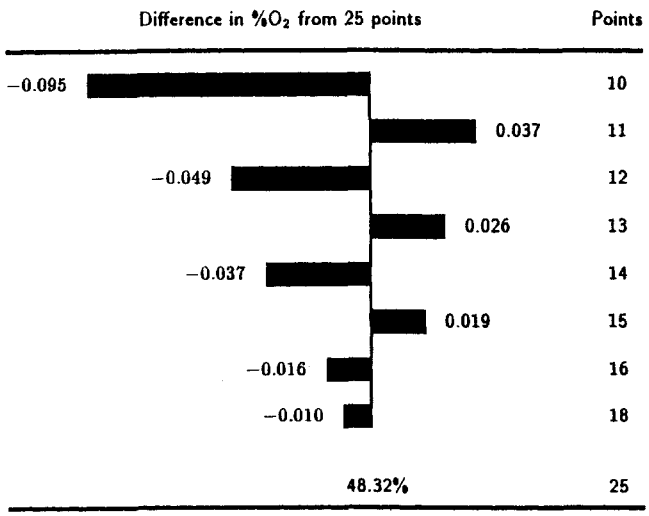

Figure 5. Difference in the steady-state oxygen concentration compared to one with 25 points for varying number of interior collocation points.

collocation points and negative for an odd number of points. This pattern has also been observed in the modeling of an adsorber using orthogonal collocation by Sristava and Joseph (1984). The Runge-Kutta-Merson explicit method was used to integrate the ODE's generated by the orthogonal collocation method with a tolerance of 1×10^{-6} with reasonable computational times (e.g., 34 s with 13 interior collocation points for the product release step of 60 s on a PRIME 750 computer which is comparable in speed to a portable 20MHz 80386 home computer). Gear's implicit method was tried but the Jacobian had to be calculated numerically as the equations were implicitly related. Difficulties encountered in calculating the Jacobian gave rise to computational times that varied by an order of magnitude or more from cycle to cycle and from step to step. It was also found that the computational time still varied with each cycle after a steady state was reached, making Gear's method unsuitable for use with this model.

Adsorption rates

The adsorption rates were obtained from isobaric breakthrough curves carried out using 21% O_2–79% N_2 mixture, pure nitrogen and pure oxygen. The PSA isobaric steps were used to simulate the breakthrough curves. Minimization of the errors in matching the predicted and experimental results were used to obtain the adsorption rates using both the adsorption and desorption data. This method has been described by Garg and Ruthven (1974). Figure 6 shows the experimental and theoretical results for the adsorption and desorption of a 21% O_2 in N_2 mixture with pure oxygen. The adsorption rates obtained were $k_{O_2} = 0.30\ s^{-1}$ and $k_{N_2} = 0.15\ s^{-1}$.

The model was shown to be much more sensitive to the nitrogen adsorption rate than to the oxygen adsorption rate and the ratio of k_{O_2}/k_{N_2} is 2:1. Daly and Granville (1980) reported that the diffusivities of oxygen in Laporte 5A zeolite crystals were approximately twice as fast as the diffusivity of nitrogen. In the PSA model proposed, the mass transfer processes that occur in the zeolite crystals have been brought together in this model using an overall adsorption rate parameter which involves the transport of adsorbate within the intracrystalline channels in the

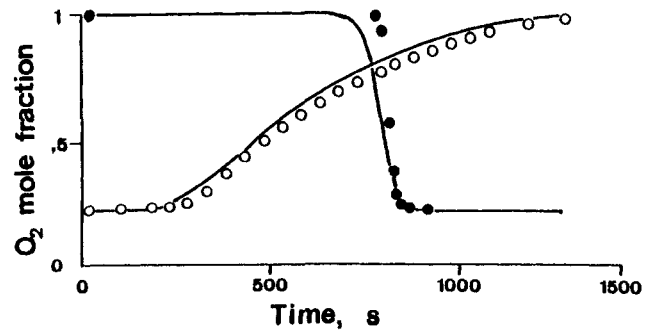

Figure 6. Theoretical (line) and experimental breakthrough curves for the adsorption and desorption of a 21% O_2–79% N_2 mixture and pure oxygen.

micropore region. The ratio of k_{O_2}/k_{N_2} suggests that, for zeolite 5A, the intercrystalline transport processes do play an important role in determining the separation of gas mixtures by PSA. Garg and Ruthven (1974) reported that for a Linde type 5A zeolite, the micropore resistance was the dominant resistance in the adsorption of nitrogen which supports the observation from the breakthrough curves.

The backfill cycle

Experimental. Figure 7 shows the averaged oxygen concentration obtained in the product at steady state for the conditions given in Table 2 (configuration B1). The oxygen concentration at steady state was first averaged over each cycle and these values for a large number of cycles were then averaged. The aver-

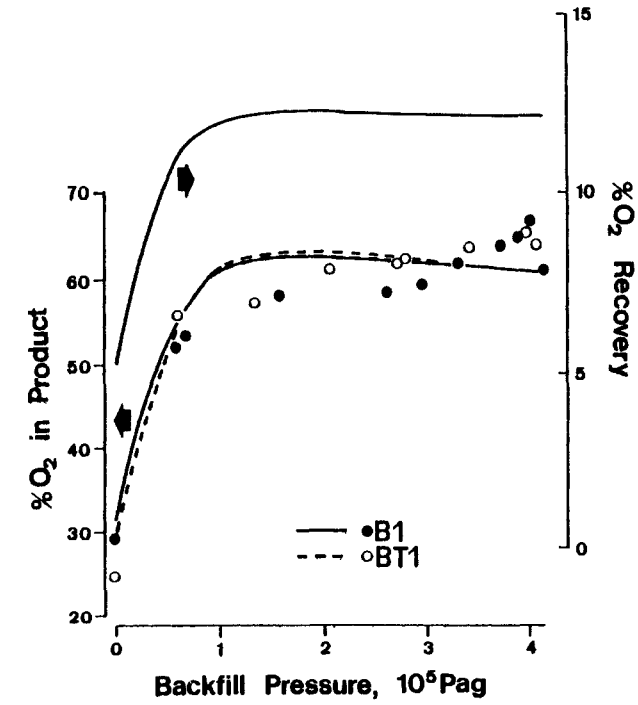

Figure 7. Theoretical and experimental steady-state product oxygen concentration together with predicted oxygen recovery as a function of the backfill pressure.

Table 2. Conditions of the Experimental and Theoretical Runs in Figure 7

Pressurization rate, kPa·s^{-1}	13.8
Depressurization rate, kPa·s^{-1}	13.8
Backfill rate, kPa·s^{-1}	6.9
Product rate, m^3·s^{-1}	1.7×10^{-5}
Cycle period, s	150
Product release period, s	150
Upper operating pressure, kPa	515
Lower operating pressure, kPa	101
Temperature, K	293
k_{O_2}, s	0.30
k_{N_2}, s	0.15
Number of interior collocation points	13
Tolerance	1×10^{-6}

age oxygen concentration obtained had a standard deviation of ±0.6% O_2. The backfill cycle shows three distinct regions for the product oxygen concentration as a function of the backfill pressure. Between 0 to 130 kPag backfill pressure, the product oxygen concentration rose rapidly with increasing backfill pressure. Between 130 to 370 kPag backfill pressure, the oxygen concentration does not vary much with the backfill pressure. Between 370 to 410 kPag pressure, an unsteady-state region was found where the oxygen concentration fluctuated substantially, rising initially in value and then falling rapidly above 390 kPag. The product oxygen concentration fell rapidly over the last 10 kPa of backfill pressure. The first two regions have been reported by Kirkby (1983); however, the unsteady region was not studied carefully by Kirkby as he encountered mechanical problems with his apparatus in that region. The unsteady region was characterized by a varying product oxygen concentration which oscillated over 20–40 cycles. The results in Figure 7 represent an averaged concentration over 150 cycles. The fluctuations suggest that the process may be chaotic over this backfill pressure range as theoretical simulations with the proposed model given later shows little changes in the bed concentration profile and steady-state concentrations in the backfill pressure range of interest. We suggest that further work should be carried out to study this region.

The results for a backfill cycle with the pressurization occurring together with the product release step (configuration BT1) showed no substantial difference in the product oxygen amount over most of the range of backfill pressures used. At zero backfill pressure, there is no backfill step to form an oxygen-rich zone within the bed. The pressurization step alone forms the oxygen-rich zone within the bed which can then be released during the product release step. Configuration BT1 gave an oxygen concentration of 25% O_2 against 29.3% O_2 for configuration B1 showing that the pressurization step is crucial at zero backfill pressure, and this is in agreement with the findings of Flores-Fernandez and Kenney (1983). This difference is significant because the enrichment is low at zero backfill pressure. Hence, for a simple cycle, the formation of a high oxygen concentration front is crucial to the product oxygen concentration obtained, and the omission of a separate pressurisation step is detrimental to the cycle's performance. The addition of the backfill step replaces much of the functions of the pressurization step in that the high oxygen concentration front is formed at the center of the bed during the backfill step. The pressurization step then needs only to push the front towards the product end. Figure 7 shows that a separate backfill step is not required above a backfill pressure of 50 kPa as the product oxygen concentration of the two configurations studied are similar.

Theoretical Results. The theoretical results (Figure 7) show good agreement with the experimental results, the best around 0 to 200 kPag backfill pressure where the sharp rise in oxygen concentration and subsequent plateauing occurs. Above 200 kPag backfill pressure, the theory predicts a small decrease in the product oxygen concentration with increasing backfill pressure. The theoretical results deviate at most from the experimental values by 8% after accounting for the presence of argon. This agreement is good as a number of experimental factors have not been accounted by the theory and they include the dead volumes in the piping, the effect of the heat of adsorption, the variation in ambient temperature, and the valve flow characteristics. The unsteady region (370 to 410 kPag backfill pressure) is not predicted by the theory. The cause of the fluctuations in oxygen concentration in this region may be due to thermal and piping effects. Farooq et al. (1988) have shown that in the nonisothermal PSA separation of ethylene-helium mixtures, the effect of temperature can lead to different steady states depending on the starting conditions. It may be possible that the nonlinearities in the physical process give rise to sudden changes in oxygen concentration.

The theory predicts that configuration BT1 performs as well as configuration B1 above 50 kPag backfill pressure as is supported by the experimental results. Between 0 to 100 kPag backfill pressure, the theory predicts that configuration B1 gives a slightly higher product oxygen than configuration BT1. The largest difference occurs at 0 kPag backfill pressure, where the experiments give a 4.3% O_2 concentration difference while the theory predicts a 2% O_2 concentration difference. Between 100 to 410 kPag backfill pressure, the theory predicts that the configuration BT1 gives a slightly higher product oxygen concentration than configuration B1. This small difference cannot be observed experimentally as it is smaller than the accuracy obtainable from the oxygen meter. The theory, in agreement with the experimental results, shows that the backfill step can be used to replace a separate pressurization step.

The calculated oxygen recovery curve shows a similar trend to that of the oxygen concentration curve. No substantial differences were noted in the recoveries between configuration B1 and BT1. Due to difficulties in obtaining reliable estimates of the cumulative gas flows in and out of the bed resulting from the large changes in transient gas velocities, no experimental data were available on the oxygen recovery. Configuration BT1 can have a shorter cycle than the corresponding B1 as the pressurization and product release cycles are merged. Without the null step, the shorter cycle time gives BT1 a higher productivity per unit adsorbent per unit time by up to 10% indicating that configuration BT1 should be used in preference to B1 in commercial units.

Concentration profiles in the bed

Figure 8 shows the bulk gas-phase oxygen concentration profiles in the bed for the end of the depressurization, backfill, pressurization and product release steps at steady state for a number of different backfill pressures for configuration BT1. The oxygen concentration profile for the null step is not reproduced as it is similar to that of the depressurization step.

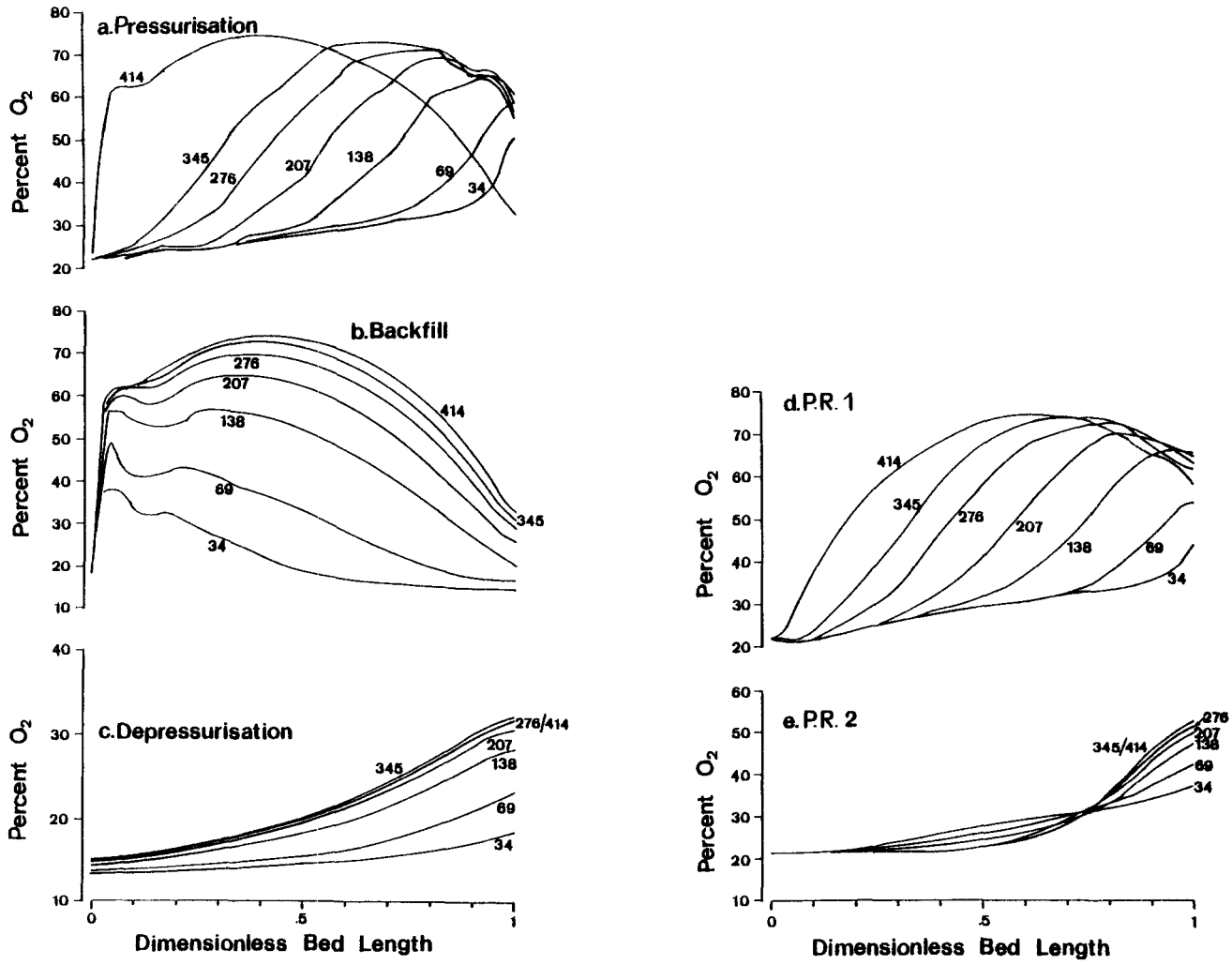

Figure 8. Predicted bulk gas-phase oxygen concentrations at the end of different steps in the backfill cycle for configuration BT1.

P.R. 1 denotes the product release step before releasing product for backfilling. P.R. 2 denotes the product release step after backfilling is completed. The numbers on the curves are the backfill pressure in kPag.

Depressurization. The oxygen profile at the end of the depressurization step gets progressively steeper as the backfill pressure increases. The oxygen profile changes rapidly between 30 to 130 kPag backfill pressure. This coincides with the steep change in product oxygen concentration with backfill pressure as shown in Figure 7. The rate of change in the oxygen profile decreases rapidly between 180 to 410 kPag backfill pressure. At the end of the product release step, a high oxygen front is left at the product end ($Z = 1$) of the bed. This high oxygen front acts as a purge stream when it moves towards the ($Z = 0$) end of the bed during the pressurisation step. The high oxygen front is inadequate to fully purge the bed as Kirkby and Kenney (1987) showed that, for the optimum regeneration of the bed, the bed at $Z = 0$ should have an oxygen concentration equal to the feed oxygen concentration before a pressurization or backfill step is initiated. This suggests that the use of a purge step, which is outside the scope of this study, at the end of the depressurization step would enhance both the product oxygen concentration and the oxygen recovery. The oxygen profiles also show that between 250 to 410 kPag backfill pressure, the regenerated bed has similar oxygen concentration profiles.

Backfill. In the backfill step, part of the product stream is fed into the bed through the product end ($Z = 1$) to repressurize the bed. The feed for the backfill step sees a decreasing gas-phase oxygen concentration as it moves down the bed and an oxygen concentration front is formed which is diffused by the effects of axial dispersion and mass transfer resistance. It can be seen that the profile for the oxygen concentration front is steep near the region of $Z = 0$ to $Z = 0.05$. The steepness of the oxygen concentration front increases rapidly for backfill pressures between 30 to 100 kPag, but changes slowly for higher backfill pressures between 120 to 410 kPag.

For the 30 to 200 kPag backfill pressure cases, there are two maximums in the oxygen concentration profile. The first maximum near $Z = 0$ arises from the oxygen concentration front caused by the feed gas pushing the oxygen initially present in the bed at the $Z = 1$ end towards the $Z = 0$ end. The second maximum around $Z = 0.2$ is brought about by the change in oxygen concentration of the backfill feed. The backfill feed for the 30–150 kPag backfill pressure cases decreases with time, and this produces the second oxygen concentration front. For the 200 to 410 kPag backfill pressure cases, the feed into the bed

initially increases and then decreases. Initially the feed is at a high concentration and it creates a diffusing front which merges with the first maximum to form an oxygen concentration profile with only one maximum. The position of the maximum moves from around $Z = 0.38$ to $Z = 0.42$ over the 200 to 410 kPag backfill pressure range. The largest change in oxygen concentration over the whole bed occurs over the 30 to 180 kPag backfill pressure range, the rate of change decreases rapidly over the 180 to 410 kPag backfill pressure range.

Pressurization. In the pressurization step, the feed is fed through the feed end at $Z = 0$ while product is withdrawn at $Z = 1$. For the 34 and 69 kPag backfill pressure cases shown in Figure 8, the amount of feed gas in the pressurization step is much larger than that in the backfill step. As the feed gas is at a fixed oxygen concentration which is lower than the maximum oxygen concentration in the bed, the oxygen front in the bed is pushed towards the product end ($Z = 1$) forming a high oxygen concentration front. The large amount of feed gas causes the oxygen concentration front to be pushed right to the product end whereby the front merges with the maximum left behind after the backfill step. For the 70 to 410 kPag backfill pressure cases, the ratio of the amount of feed gas in the pressurization step to that in the backfill step decreases with increasing backfill pressure. Although the pressurization step increases the value of the oxygen concentration maximum, it is unable to push the oxygen concentration front far enough to create a maximum at the product end. Moreover, for the 210 to 390 kPag backfill pressure cases, the bed has two oxygen concentration maximums at the start of the step. The incoming oxygen feed further develops the first oxygen concentration front present near $Z = 0$ and pushes the front towards the product end ($Z = 1$). However, it does not push the first front enough to merge with the second oxygen concentration maximum, so that two maximums are still left in the bed at the end of the step. For the 35 to 390 kPag backfill pressure cases, the oxygen concentration maximums lie between $Z = 0.7$ to 1. For the 410 kPag backfill pressure case, there is no pressurization step and the maximum oxygen concentration lies at $Z = 0.4$. Therefore, over the 390 to 410 kPag backfill pressure range, the position of the highest maximum oxygen concentration moves from $Z = 0.7$ to $Z = 0.4$, and this accounts for the theoretical drop in oxygen concentration in the product. However, it does not explain the sudden increases in oxygen concentration in the product as measured experimentally.

Product Release. Two oxygen profiles for the product release step are presented in Figure 8. The first figure (8d) shows the oxygen profiles in the bed before part of the product is being used for backfilling the second bed; the second figure (8e) shows the oxygen profiles at the bed after backfilling has been completed. Before backfilling, the product release step moves only a small part of the high oxygen front into the product stream. For backfill pressures between 130 and 410 kPag, it is during the product release for backfilling that the oxygen maximum is moved out of the bed. This effectively moves a large fraction of the oxygen between the two beds giving the oxygen a longer residence time which enhances the product concentration and recovery. At the end of the product release step, the high oxygen concentration front has been moved out of the bed, and the oxygen profiles are similar in shape to that of the depressurization step.

Table 3. Sensitivity Analyses of the Backfill Step

Base Case Parameter	Effect	Product % Oxygen 62.48%		% Oxygen Recovery 12.20%	
		Change	% Change	Change	% Change
Upper operating pressure	+10%	0.78	1.26	−0.80	−6.57
	−10%	−1.31	−2.09	0.94	7.66
Backfill rate	+10%	0.67	1.07	0.13	1.04
	−10%	−1.52	−2.43	0.47	3.89
Langmuir isotherm $C_T O_2$	+10%	−6.71	−9.78	−1.37	−11.29
	−10%	6.09	9.75	1.43	11.73
Langmuir isotherm $C_T N_2$	+10%	7.07	11.32	0.66	5.39
	−10%	−8.33	−13.34	−0.97	−7.94
Bed length	+10%	0.99	1.59	−0.89	−7.28
	−10%	−1.16	−1.86	1.04	8.32
Effective diffusivity	+10%	−0.03	−0.04	−0.01	−0.03
	−10%	0.03	0.04	0.01	0.03
Oxygen Knudsen diffusivity	+10%	0.09	0.15	0.01	0.05
	−10%	−0.10	−0.17	−0.01	−0.06
Nitrogen Knudsen diffusivity	+10%	−0.09	−0.15	−0.01	−0.05
	−10%	0.10	0.17	0.01	0.06
Particle radius	+10%	−0.35	−0.56	−0.07	−0.57
	−10%	0.37	0.60	0.07	0.70
Oxygen adsorption rate	+10%	−0.23	−0.37	−0.04	−0.31
	−10%	0.29	0.46	0.05	0.39
Nitrogen adsorption rate	+10%	1.37	2.19	0.25	2.04
	−10%	−1.51	−2.42	−0.28	−2.26

Sensitivity analysis

Sensitivity analysis was carried out on a number of parameters used in developing the theory. The parameters chosen were those which could be varied in the design of either the PSA process or the adsorbent. Table 3 shows the effect on the product oxygen concentration and recovery when a number of parameters are varied by ±10%. Table 4 lists the conditions of the base case which is used for comparison. Changes in the Langmuir isotherm parameter, C_T, for both oxygen and nitrogen gave rise to significant changes in both product oxygen concentration and recovery. Since oxygen is to be recovered, a decrease in C_T for oxygen and an increase in C_T for nitrogen is favorable for the process. In the Langmuir analysis, C_T represents the saturation limit of the adsorbent. If C_T can be decreased for oxygen and increased for nitrogen, then the separation factor ratio for a given pressure and gas-phase composition, given by $C_{T,N_2}/C_{T,O_2}$ will be increased leading to enhanced separation between the two components. Recovery is affected much more when the C_T of oxygen is changed than when the C_T of nitrogen is changed as oxygen is adsorbed much less than nitrogen, from which it can be seen that the adsorption capacity of different gases on the adsorbent is an important parameter in determining whether a process is commercially viable or not.

The effect of changing the oxygen adsorption rate is much smaller than the corresponding change in the nitrogen adsorption rate because nitrogen is adsorbed in much larger quantities by the zeolite adsorbent and has a lower adsorption rate. Of all the parameters, the adsorption rate and diffusivities are the least sensitive to changes in their value. This lower sensitivity was also noted by Yang and Doong (1985) in their work on the separation of a CH_4—H_2 mixture. This allows a much larger variation in their values before the PSA process is markedly affected; as these parameters are difficult to control in the zeolite manufacturing process, it is therefore preferable to use the other parameters listed in Table 3 to obtain better control of the PSA process; the extent of use would, however, be governed by economic factors.

Further theoretical results

Simulations based on the zeolite 5A were carried out on the variation of the pressurization rate, product release rate, and backfill rate to study their effect on the product oxygen concentration at steady state. The results are shown in Figure 9 where the curve A corresponds to that in Figure 7.

Effect of Pressurization Rate. Curves B and C correspond to an increase in the rate of pressurisation to 27 and 69 kPag · s^{-1},

Table 4. Conditions for the Base Case in the Sensitivity Analyses

Configuration	B1
Pressurization time, s	30
Product release time, s	150
Depressurization time, s	30
Null time, s	30
Backfill time, s	30
Product rate, $m^3 s^{-1}$	1.7×10^{-5}
Backfill pressure, kPag	138
Rate of pressurization, kPa·s^{-1}	14
Rate of depressurization, kPa·s^{-1}	14
Rate of backfill, kPa·s^{-1}	7

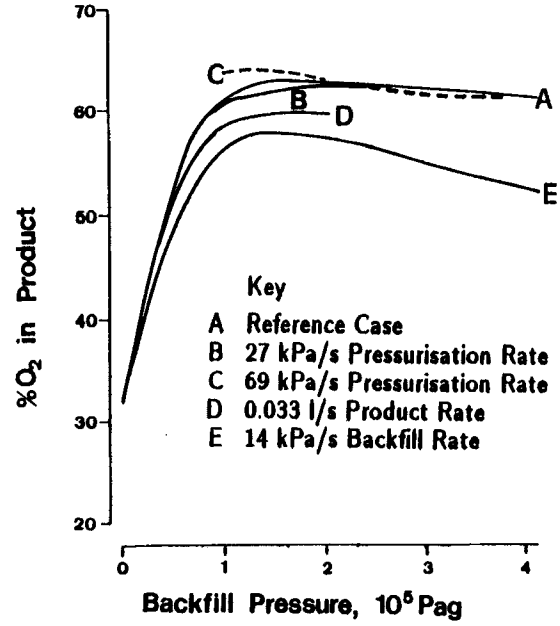

Figure 9. Comparison of the predicted effect of pressurization rate, backfill rate and product rate on the product oxygen concentration for the backfill cycle against the base case of Figure 7 and Table 2.

respectively. The simulation predicts that the effect of pressurization rate on the product oxygen concentration is small and would not be detected experimentally. Curve C gives a higher oxygen product concentration than curves A or B, which is brought about by the faster pressurization step pushing a much steeper oxygen front towards the product end because, at lower pressurisation rates, the oxygen front is diffused by axial dispersion. There is no simulated results for curve C between 0 and 100 kPag backfill pressure as the pressurisation rate is too high and the differential equations were too stiff for the integration routine used. Moreover, the changes in bed pressure along the bed will not be uniform at such a high pressurization rate, giving rise to a physical situation not covered by the theory. There is little change in curves A and B because the product release step is fairly long and the product flow rate is small, allowing the bed to come to equilibrium.

Effect of Product Rate. Curve D is for a product rate of 0.033 L · s^{-1}, twice that of curve A. The product amount per cycle is kept constant, so the period of the product release step is reduced to 75 s resulting in the maximum backfill pressure possible being 205 kPag. An increase in the product flow rate decreases the product oxygen concentration. With a higher product flow rate, the high oxygen concentration front is moved out of the bed faster and there is less time for the adsorbent phase to reach an equilibrium with the particle phase after the pressurization step has been completed. The decrease in product oxygen concentration varies between 0.2 to 3.2% O_2 over the range of backfill pressures simulated.

Effect of Backfill Rate. Curve E shows the effect of an increase in backfill rate from 6.9 to 13.8 kPa · s^{-1}. The decrease in product oxygen concentration is very marked, increasing with backfill pressure. A maximum decrease of 9.2% O_2 is observed at 410 kPag backfill pressure. A pronounced optimum is

formed. The optimum backfill pressure occurs at 140 kPag for 13.8 kPa · s^{-1} backfill rate. In comparison, the start of the plateau region occurs at 210 kPag for 6.9 kPa · s^{-1} backfill rate given by curve A.

Of the three process rates studied here, the backfill rate gives the largest decrease in product oxygen concentration followed by the product release rate. The rate of pressurization only affects the process slightly.

Effect of Particle Size. The effect of particle size on the product oxygen concentration is shown in Figure 10. Initially the increase in product oxygen concentration is fairly rapid as the particle size decreases but below a radius of 2.5×10^{-4} m, the increase slows down dramatically. Doong and Yang (1986) showed for the PSA separation of an equimolar H_2/CH_4 mixture, the governing parameter as to whether the pore diffusion could be neglected or not in the theoretical analyses was the parameter $D_e t_c/a^2$, where D_e is the effective diffusivity of the sorbate, t_c is the cycle time, and a is the radius of the particle. They suggested that for values of $D_e t_c/a^2 > 43$, pore diffusion could be neglected. The value of $D_e t_c/a^2$ for this simulation of the PSA separation of air is shown in Figure 10 and the values here range from 190 to 38,400; all values falling within the region of $D_e t_c/a^2 > 43$. When pore diffusion becomes negligible, the separation process tends towards an equilibrium model and the product oxygen concentration is independent of particle size. The results obtained suggest that a value of $D_e t_c/a^2 > 1{,}000$ is required for the effect of pore diffusion to be negligible for our case. Kirkby (1983) has shown that the use of an equilibrium model on the PSA separation of air using the same adsorbent was unable to predict the steady-state oxygen concentration for a backfill cycle having similar cycle time, as it overpredicted the oxygen concentration up to 100%. Our model was able to predict Kirkby's experimental results giving steady-state oxygen concentration to within ±8%. The results indicate that the criteria of Doong and Yang could vary with the rates of adsorption and the nature of the PSA cycle used.

Conclusion

The backfill cycle in the PSA separation of air to produce an enriched oxygen product using a zeolite 5A molecular sieve was studied theoretically and experimentally. We showed that the adsorption rate of oxygen in the micropores of the zeolite was twice that of nitrogen. The amalgamation of the pressurization and product release steps brought about an increase in productivity of adsorbent with no detrimental effect on product concentration or recovery, indicating that the amalgamation of process steps in multibed PSA operation is a viable method for increasing productivity. The important rate parameters governing the process were the backfill rate and product release rates. The study showed that, if the adsorbent's saturation adsorption capacities could be tailored, it could lead to enhanced separation, which points to the need for further development in the manufacture and tailoring of adsorbents.

The mathematical model proposed successfully predicted the steady-state behavior of the backfill cycle of the PSA process and showed the role each individual process step played. For the adsorbent used, a smaller particle radius is required to bring about instantaneous equilibrium conditions for the cycle times used, but this cannot be achieved without moving into a regime of significant pressure drop.

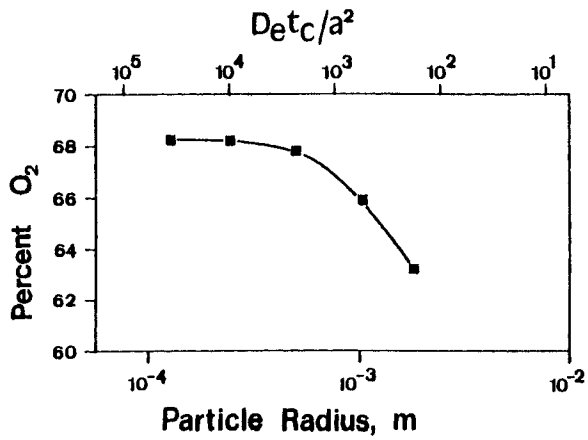

Figure 10. Effect of particle size on the product oxygen concentration for a backfill cycle with 206 kPag backfill pressure.

Acknowledgment

One of us (Liow) gratefully acknowledges financial support from the CVCP and Trinity College of Cambridge.

Notation

b = constant of the Langmuir isotherm, m^2/N
C = concentration of gas, kmol/m^3
C_T = constant of the Langmuir isotherm, kmol/kg adsorbent
d_p = particle diameter, m
D_A = axial dispersion, m^2/s
D_b = bulk diffusion coefficient in the particle, m^2/s
D_b' = bulk diffusion coefficient in the gas phase, m^2/s
D_k = Knudsen diffusion coefficient, m^2/s
i = integer
J = Flux with respect to the local molar average velocity, kmol/m^2/s
k_i = adsorption parameters, s^{-1}
K = reciprocal time constant for the experimental pressure curve, s^{-1}
L = length of bed, m
M = molecular weight
n = total number of components
N_i = flux with respect to fixed coordinates, kmol/m^2/s
N = number of interior collocation points
Pe_∞ = limiting Peclet number
P = pressure, N/m^2
$\mathcal{P}$ = Jacobi polynomial
q = concentration of adsorbed species on adsorbent surface, kmol/kg adsorbent
r = distance from centre of particle, m
R = gas constant, kg · m^2/kmol/s/K
R_o = radius of particle, m
s = mole fraction on the adsorbent surface
t = time, s
t_c = cycle time, s
t_s = step time, s
T = temperature, K
v = superficial velocity, m/s
V = volume, m^3
w = bulk density of adsorbent, kg/m^3
x = mole fraction in the particle gas phase
y = bulk gas-phase mole fraction
z = distance along the bed, m
Z = dimensionless bed distance, z/L

Greek letters

α = power of the Jacobi polynomial
β = power of the Jacobi polynomial
β' = radial dispersion factor

Δ = an infinitesimally small amount
ϵ_b = bed interparticle voidage
ϵ_p = particle voidage
ϵ_t = total bed voidage
π = spreading pressure, N/m^2
ρ_p = particle density, kg/m^3
τ = reciprocal axial tortuosity factor

Superscripts

b = bulk
D = diffusive
T = total
$*$ = equilibrium value
$\bar{}$ = particle volume averaged quantity
$^\circ$ = pure component
$+$ = a small distance upstream

Subscripts

1 = component 1
2 = component 2
f = final (Eq. 44)
i = initial (Eq. 44)
i = component i
j = component j
k = component k
s = component s
T = total

Literature Cited

Bird, R. B., W. E. Stewart, and E. N. Lightfoot, *Transport Phenomena*, Wiley, New York (1960).

Daly, W. O., and W. H. Granville, "Gas Adsorption Rate Data using Zeolitic Molecular Sieves," *The Properties and Applications of Zeolites*, R. P. Townsend, ed., *Brit. Chem. Soc.* Special Publication, No. 33, 184 (1980).

Doong, S. J., and R. T. Yang, "Parametric Study of the Pressure Swing Adsorption Process for Gas Separation: A Criterion for Pore Diffusion Limitation," *Chem. Eng. Commun.*, **41**, 163 (1986).

Farooq, S., M. M. Hassan, and D. M. Ruthven, "Heat Effects in Pressure Swing Adsorption Systems," *Chem. Eng. Sci.*, **43**, 1017 (1988).

Flores-Fernandez, G., and C. N. Kenney, "Modelling of the Pressure Swing Air Separation Process," *Chem. Eng. Sci.*, **38**, 827 (1983).

Garg, D. R., and D. M. Ruthven, "The Performance of Molecular Sieve Adsorption Columns: Systems with Micropore Diffusion Control," *Chem. Eng. Sci.*, **29**, 571 (1974).

Jackson, R., *Transport in Porous Catalyst*, Chemical Engineering Monograph 4, Elsevier, New York (1977).

Kayser, J. C., and K. S. Knaebel, "Integrated steps in pressure swing adsorption cycles," *Chem. Eng. Sci.*, **43**, 3015 (1988).

Kirkby, N. F., "Pressure Swing Gas Separation," PhD Diss., University of Cambridge (1983).

Kirkby, N. F., and C. N. Kenney, "The Role of Process Steps in Pressure Swing Adsorption," *Fund. of Adsorption*, Engineering Foundation, New York, 319 (1987).

Langer, G., A. Roethe, K. P. Roethe, and D. Gelbin, "Heat and Mass Transfer in Packed Beds: III. Axial Mass Dispersion," *Int. J. Heat Mass Transfer*, **21**, 751 (1978).

Liow, J. L., "Air Separation by Pressure Swing Adsorption," PhD Diss., University of Cambridge (1986).

Myers, A. L., and J. M. Prausnitz, "Thermodynamics of mixed-gas adsorption," *AIChE J.*, **11**, 121 (1965).

Ruthven, D. M., *Principles of Adsorption and Adsorption Processes*, Wiley, New York (1984).

Shin, H. S., and K. S. Knaebel, "Pressure Swing Adsorption: A Theoretical Study of Diffusion-Induced Separations," *AIChE J.*, **33**, 654 (1987).

———, "Pressure Swing Adsorption: An Experimental Study of Diffusion-Induced Separation," *AIChE J.*, **34**, 1409 (1988).

Skarstrom, C. W., "Method and Apparatus for Fractionating Gaseous Mixtures by Adsorption," U.S. Patent 2944627 (1960).

———, "Heatless Fractionation of Gaseous Materials," U.S. Patent 3104162 (1963).

Sorial, G. A., "Binary Gas Adsorption on Molecular Sieves," PhD Diss., University of Bradford (1982).

Sristava, R. K., and B. Joseph, "Simulation of Packed-bed Separation Processes using Orthogonal Collocation," *Comp. & Chem. Eng.*, **8**, 43 (1984).

Villadsen, J., and M. L. Michelsen, *Solution of Differential Equation Models by Polynomial Approximation*, Prentice-Hall, Eaglewood Cliffs, NJ (1978).

Wankat, P. C., *Large-Scale Adsorption and Chromatography: II*, CRC Press, Boca Raton, FL (1986).

Yang, R. T., *Gas Separation by Adsorption Processes*, Butterworths, Stoneham, MA (1987).

Yang, R. T., and S. J. Doong, "Gas Separation by Pressure Swing Adsorption: A Pore-Diffusion Model for Bulk Separation," *AIChE J.*, **31**, 1829 (1985).

Manuscript received Mar. 11, 1989, and revision received Oct. 2, 1989.